Ultrasonics 99 (2019) 105955

Contents lists available at ScienceDirect

Ultrasonics

journal homepage: www.elsevier.com/locate/ultras

Visualization of the interaction of guided acoustic waves with water by light refractive vibrometry

Sabrina Tietze*, Gerhard Lindner

Institute of Sensor and Actuator Technology, Coburg University of Applied Sciences and Arts, Am Hofbrauhaus 1b, 96450 Coburg, Germany

ARTICLE INFO

Keywords:
Guided acoustic waves
Light refractive vibrometry
Quasi-Scholte plate modes
Lamb waves

ABSTRACT

Guided acoustic waves, such as Lamb waves, are widely applied for material characterization, sensing of liquids and the generation of streaming in liquids. There are numerical simulation tools for the prediction of their propagation near a solid-liquid boundary but a demand for complementary measurement techniques for the validation of the simulation results remains. In this contribution it is demonstrated that light refractive vibrometry is a suitable approach for the visualization of the interaction of guided acoustic waves with liquids. For this purpose Lamb waves were excited by piezoelectric transducers on copper plates partially immersed in water. There the fundamental symmetric and antisymmetric modes are converted to compressional waves and quasi-Scholte plate waves below a frequency-thickness product of 1 MHz mm. From the vibrometry scans the wavelengths, radiation angles and pressure amplitudes of the involved modes could be determined and thus theoretical predictions of the attenuation of the Lamb modes and the energy distribution of quasi-Scholte plate waves between the solid substrate and the liquid environment could be confirmed.

1. Introduction

The excitation of guided acoustic waves on non-piezoelectric solid substrates by piezoelectric transducers is a well established technique for strutural health monitoring or remote sensing [1–4]. By immersing such acoustic waveguides into liquids it is possible to sense liquid properties or coatings on the substrate surface [3–6]. Furthermore they allow the remote generation of acoustic streaming in liquids [7–9]. The propagation of guided acoustic waves at solid-liquid boundaries, however, differs substantially from their behavior in a gaseous or vacuum environment. In contrast to solid-gas boundaries, the guided waves on solid-liquid boundaries may suffer from radiation losses due to mode conversion into compressional waves in the liquid or may be converted into quasi-Scholte plate modes (QSP) or Scholte waves [10–14]. In particular with respect to the influence on transport processes across liquid-solid boundaries by guided acoustic waves such as the enhancement of ion transport at electrodes in an electrochemical cell [9,15,16], a detailed understanding of the interaction of these waves with the liquid surrounding is desired. There are powerful tools for numerical simulations commercially available, such as DISPERSE, but a correspondingly effective measurement technique was missing to a large extent up to now. For the characterization of guided acoustic waves at solid-air interfaces the laser Doppler vibrometer (LDV) is a well established measurement tool [17,18]. Up to now schlieren optical measurements [19,20,14] or measurements with hydrophones [21–24] were carried out for their characterization at solid-liquid interfaces. These approaches, however, suffer from specific limitations. In hydrophone measurements, where the PVDF membrane hydrophone itself disturbs the medium and hinders the propagation of the sound wave or measurements immediately neighboring the solid-liquid interface are impossible because of the extension of the hydrophone and capacitive crosstalk. Schlieren optical measurements are also suitable for measurements near the solid-liquid interface, but the proper adjustment of the optical components, which is necessary for the desired high sensitivity, is very time-consuming. The most promising measurement system is the LDV. Meanwhile commercially available systems are mostly scanning laser Doppler vibrometers (SLDV). Thus the time of adjustment of the optical components is short and a spatial measurement area can be scanned. Unfortunately the measurement effect is based on the component of the displacement in the direction of the incident laser beam. Therefore, shear-horizontal waves are only detectable when the laser beam is inclined with respect to the surface and more than one scan head is used [17]. An inclined beam is also recommended for fundamental symmetric Lamb modes with significant in-plane displacements. In our approach light refractive vibrometry (LRV) is used for the analysis of guided acoustic waves in liquid

* Corresponding author.
E-mail address: sabrina.tietze@hs-coburg.de (S. Tietze).

https://doi.org/10.1016/j.ultras.2019.105955
Received 19 March 2019; Received in revised form 15 June 2019; Accepted 28 June 2019
Available online 15 July 2019

environment. This allows the detection of the propagation of sound waves in liquids. Up to now this method is predominantly applied for the measurement of sound waves in air caused by the emission from an ultrasonic probe [25–28], but a few authors described its application to liquid media as well [29–34]. First measurements in context with guided acoustic waves are done by Tietze et al. [6] for the characterization of radiated waves in a liquid-filled tube. In the present study we want to show that it is possible to visualize the interaction of guided acoustic waves with liquids with LRV. We used copper plates partially immersed in water as waveguides, on which Lamb waves were excited by piezoelectric transducers attached to the non-immersed part. We report on the visualization and the quantitative analysis of the wave modes propagating along and in the neighborhood of the immersed part of the waveguide at different frequencies and compare the results with numerical calculations performed with DISPERSE. Finally a comprehensive understanding of the propagation of Lamb waves on a waveguide immersed in a liquid and the conversion of wave modes into compressional waves in the liquid and QSP modes was obtained.

2. Theoretical background

Both the numerical calculations and the interpretation of the observations are based on the established theoretical model of Lamb wave interaction with liquids resulting in QSP modes or Scholte waves [3,1,35,36], which is summarized in this section. In addition, the functional principles of LDV and LRV are explained therein.

2.1. Guided acoustic waves

For convenience only plane waves propagating along a plate of thickness $2 \cdot h$ in x-direction are considered. The normal displacement of the wave follows the z-direction. Our starting points are the potential functions Φ and Ψ for the longitudinal and transverse modes of plate waves (Lamb waves):

$$\Phi = \Phi(z)e^{i(kx-\omega t)} = [A_1\sin(pz) + A_2\cos(pz)]e^{i(kx-\omega t)}\,\Psi = \Psi(z)e^{i(kx-\omega t)} = [B_1\sin(qz) + B_2\cos(qz)]e^{i(kx-\omega t)} \tag{1}$$

with k the wave number, t the time, $\omega = 2\pi f$, f the frequency, $p^2 = \frac{\omega^2}{c_l^2} - k^2$ and $q^2 = \frac{\omega^2}{c_t^2} - k^2$, c_l and c_t the longitudinal and transverse sound velocities of the plate material. A_1, A_2, B_1, B_2 are arbitrary variables depending on the boundary conditions. The displacement functions u_x and u_z and the stress functions σ_{zx} and σ_{zz} of the wave can thereby be calculated by:

$$u_x = \frac{\partial\Phi}{\partial x} + \frac{\partial\Psi}{\partial z} u_z = \frac{\partial\Phi}{\partial z} - \frac{\partial\Psi}{\partial x} \sigma_{zx} = \mu\left(\frac{\partial u_z}{\partial x} + \frac{\partial z_x}{\partial z}\right) \sigma_{zz} = \lambda\left(\frac{\partial u_x}{\partial x} + \frac{\partial u_z}{\partial z}\right) + 2\mu\frac{\partial u_z}{\partial z} \tag{2}$$

where λ and μ are the Lamé constants of the plate. In vacuum or air the boundary conditions $\sigma_{zx} = \sigma_{zz} = 0$ apply at $z = \pm h$. It is known that the solutions can be divided into symmetric and antisymmetric modes of the plate.

If the plate is immersed in a liquid, the potential of the liquid is also to be taken into account. This potential is assumed to be an ideal non-viscous fluid, i. e. without shear components. Thus the liquid has only the potential Φ_f which is defined by:

$$\Phi_f = A_f e^{-k_f p_f z} e^{i(kx-\omega t)} \tag{3}$$

with $p_f = \sqrt{\left(\frac{c_f}{c_{ph}}\right)^2 - 1}$, c_{ph} the phase velocity of the guided wave and c_f the sound velocity of the liquid. Correspondingly, at $z = \pm h$ the boundary conditions change into $\sigma_{zx} = \sigma_{zx}^f$ and $\sigma_{zz} = \sigma_{zz}^f$ and the following equation systems can be established for the symmetric, Eq. 4, and antisymmetric modes, Eq. 5:

$$\begin{bmatrix} -2ikp\sin(ph) & (k^2-q^2)\sin(qh) & 0 \\ [-\lambda(k^2+p^2) - 2\mu p^2]\cos(ph) & -2\mu ikq\cos(qh) & -\rho_f\omega^2 k_f p_f e^{-k_f p_f h} \\ -p\sin(ph) & -ik\sin(qh) & k_f p_f e^{-k_f p_f h} \end{bmatrix} \begin{pmatrix} A_2 \\ B_1 \\ A_{1,f} \end{pmatrix} = \begin{pmatrix} 0 \\ 0 \\ 0 \end{pmatrix} \tag{4}$$

$$\begin{bmatrix} 2ikp\cos(ph) & (k^2-q^2)\cos(qh) & 0 \\ [-\lambda(k^2+p^2) - 2\mu p^2]\sin(ph) & 2\mu ikq\sin(qh) & -\rho_f\omega^2 k_f p_f e^{-k_f p_f h} \\ p\cos(ph) & -ik\cos(qh) & k_f p_f e^{-k_f p_f h} \end{bmatrix} \begin{pmatrix} A_1 \\ B_2 \\ A_{2,f} \end{pmatrix} = \begin{pmatrix} 0 \\ 0 \\ 0 \end{pmatrix} \tag{5}$$

with ρ_f the density of the fluid. Solving these systems of homogeneous equations with respect to the unknown variables A_1, A_2, B_1, B_2, $A_{1,f}$ and $A_{2,f}$ ends up with dispersion relations for the phase velocity as a function of the frequency-thickness product. For real frequencies complex solutions of the wavenumber will be obtained. Thereby the real part corresponds to the phase velocity and the imaginary part represents the attenuation of the wave by radiation into the surrounding liquid. Consequently, for phase velocities c_{ph} faster than the sound velocity of the fluid c_f, the wave will leak into the liquid with an angle Θ given by:

$$\sin\Theta = \frac{c_f}{c_{ph}} \tag{6}$$

which is called Lamb angle. The radiated wave in the liquid propagates as a compressional wave. Besides those solutions with complex wavenumbers, however, also solutions with purely real wavenumbers exists. The phase velocities of these waves are slower than the sound velocity of the liquid. Therefore they do not radiate into the liquid, but remain tethered to the substrate. Such solutions represent non-dispersive Scholte waves at higher values of the frequency-thickness product and dispersive QSP modes at lower values.

2.2. Laser Doppler vibrometry and light refractive vibrometry

The functional principle of a laser Doppler vibrometer is based on the Mach-Zehnder-Doppler interferometer [37]. A reference beam and the measuring beam are divided by a beam splitter. The measurement beam is reflected by the surface of the vibrating sample and will propagate to the detector along varying path lengths. The reference beam, on the other hand, has a fixed propagation distance directly to the detector. The measurement of the vibration velocity of the sample is based on the Doppler effect of the measurement beam, i. e. its frequency is shifted by f_D dependent on the velocity v_S of the sample and the original wavelength λ_L of the wave by

$$f_D = \frac{2v_S}{\lambda_L}. \tag{7}$$

The intensity I_{tot} measured at the detector is determined by the interference of reference and measurement beam and is calculated from the respective intensities I_1 and I_2 by

$$I_{tot} = I_1 + I_2 + 2\sqrt{I_1 I_2}\cos\left[\frac{2\pi(L_1 - L_2)}{\lambda_L}\right], \tag{8}$$

where L_1 and L_2 represent the different path lengths. Thus the vibrational modulation of the path length of the measurement beam and its interference with the reference beam produces a light-dark pattern on the detector. One light-dark cycle corresponds to half a wavelength of the laser. By means of an acousto-optical modulator (Bragg cell), which produces a permanent frequency shift of 40 MHz, the movement direction of the object can be obtained as well. For the measurement of

the displacement instead of the velocity of the object, not the Doppler frequency shift is used but the light-dark transitions are counted. However, only the displacements perpendicular to the measurement beam can be detected in this way.

In contrast to the conventional LDV, by LRV not the movement of the reflective object is measured. But changes of the optical path length L in the transmitted medium caused by variation of its refractive index n compared to the physical path length L_p are registered:

$$L(t) = 2\int_0^{L_p} n(y, t)dy. \tag{9}$$

Such changes of the refractive index of liquids can be caused by the pressure variations of sound waves. Correspondingly an apparent variation of the optical path length happens without any movement of the reflecting object (reflector). In this way the sound pressure field resulting from the interaction of the guided acoustic wave with the liquid becomes visible. According to Bahr and Lerch [29], the change of the refractive index n due to the pressure variations in the liquid is described by the following equation:

$$n(x, y, t) = n_0 + \left(\frac{\partial n}{\partial p}\right)_S p(x, y, t) \tag{10}$$

where n_0 is the ambient refractive index of the medium and $\left(\frac{\partial n}{\partial p}\right)_S$ is the piezo-optical coefficient, which is specified by Scruby and Drain [38] for water at an optical wavelength of 633 nm to be $1.444{\cdot}10^{-10}\frac{1}{Pa}$ at 25 °C.

3. Materials and methods

The experiments are performed with elongated copper plates with a width of 25 mm and thicknesses of 0.5 mm and 1 mm. Guided acoustic waves are excited on these plates by piezoelectric transducers glued with an epoxy adhesive near one end of the copper plate. Different dimensions of piezoelectric transducers were chosen in order to generate waves at different frequencies and thereby of different wavelengths. Because of the dispersive character of the guided acoustic waves it was expected that the pressure field in the liquid would change with frequency. The sample configurations and frequencies chosen in the experiments are compiled in Table 1. In the first step a single point measurement with the SLDV (PSV 400M, Polytec GmbH, Waldbronn, Germany) perpendicular to the copper plate is performed in air. Therefore the laser beam of the SLDV is focused directly in front of the copper surface in air at a spot 1 cm distant from the lower end of the plate. A five-cycle tone burst is amplified by an amplifier (PA120A, WME Power Systems GmbH, Hamburg, Germany) and a voltage doubler to generate voltages from 10 Vpp up to 105 Vpp at the transducer. This voltage is varied until the same perpendicular displacement was recorded by the SLDV for each configuration and frequency. The experimental set-up for the LRV is shown in Fig. 1. For the measurement a rectangular vessel is used in which the copper sample is fixed to the ground by a socket. Plane guided acoustic waves will be generated by the piezoelectric transducer outside of the liquid and propagate along the sample outside and within the liquid. Now, the laser beam is focused to a rigid reflector behind the vessel. The scan range extends around the copper sample in the liquid and begins 5 mm below the water surface. With the displacement decoder DD-300 the resolution of the minimum detectable pressure fluctuation of the LRV can be calculated by [29]:

$$p_{min} = \frac{5{\cdot}10^{-13}\,\mathrm{m}}{2{\cdot}1.444{\cdot}10^{-10}\,\mathrm{y}} = 1.73\,\frac{\mathrm{Pa}}{\mathrm{y/mm}} \tag{11}$$

where y is the width of the copper plate, because the pressure fluctuations in the liquid are assumed to happen only within this range.

Table 1
Thickness of copper samples, transducer dimensions and frequencies.

Thickness	Dimension of piezoelectric transducer	Frequency
1 mm	30 mm × 10 mm × 1 mm	60 kHz
1 mm	30 mm × 10 mm × 1 mm	190 kHz
1 mm	25 mm × 1 mm × 1 mm	620 kHz
0.5 mm	25 mm × 1 mm × 1 mm	900 kHz

4. Results

With the dispersion relations of 2.1 it is possible to calculate phase velocity diagrams of guided acoustic waves both outside and within the liquid. In Fig. 2 such diagrams for symmetrical and antisymmetrical wave modes are shown. They are calculated with the commercially available program DISPERSE Version 2.0.20a. For a copper plate in air the phase velocity diagram in Fig. 2a is valid. With the frequencies and plate thicknesses of Table 1 it is seen that only fundamental symmetric and antisymmetric modes are excitable. Whereas with increasing frequency-thickness product the phase velocity of the antisymmetrical mode increases, the phase velocity of the fundamental symmetric mode decreases. When the guided wave propagates within water two additional modes which are slower than the sound velocity of water appear, see Fig. 2b. The dispersive mode at low frequency-thickness product is called quasi-Scholte plate mode (QSP) and behaves similiar to the fundamental antisymmetric mode. It emerges into the Scholte wave for higher frequency-thickness products, which is non-dispersive and behaves similar to a Rayleigh wave [1,10,36]. The attenuation of each mode in water calculated from the imaginary part of the complex wavenumber are shown in Fig. 3a. Obviously the fundamental symmetric mode has a smaller attenuation coefficient than the fundamental antisymmetric mode up to 1.5 MHz mm. Therefore within the experimental conditions of this study it is expected that the S_0 mode propagates on the copper plate for longer distances than the A_0 mode. Besides this the sound radiation into the liquid should be more focused for the A_0 mode. Furthermore the calculated Lamb angle is shown in Fig. 3b as a function of the frequency-thickness product. From this it is expected that the S_0 mode has a smaller Lamb angle than the A_0 mode. It is also indicated in Fig. 3 that the attenuation coefficient of the QSP is zero and thereby the QSP does not radiate into the surrounding liquid because it has only real wavenumbers. The evanescent QSP waves will remain tethered to the copper substrate. In contrast the fundamental symmetric and antisymmetric modes radiate into the liquid with the angles calculated by formula 6. In Table 2 the results of the preliminary LDV measurements on copper plates in air are summarized. It contains the perpendicular displacements obtained at different values of the frequency-thickness product for an excitation voltage of 105 V_{pp} at the piezoelectric transducer. Furthermore the excitation voltages needed for a displacement of 2 nm are also listed. In all cases the fundamental antisymmetric mode exhibits higher displacements than the fundamental symmetric mode. In addition it is shown that the displacement of the fundamental antisymmetric mode decreases with increasing frequency-thickness product. The same holds for the fundamental symmetric mode except of the result at 60 kHz mm, where the mode signal could not be distinguished from the signal noise. The excitation voltage needed for a displacement of 2 nm increases monotonously with increasing frequency-thickness product. This relationship allows to adjust the excitation voltage of the transducers in the light refractive vibrometry measurements at different frequencies in such a way that always the same perpendicular displacement of the A_0 mode is achieved before entering the liquid. In the following results obtained with LRV measurements in the liquid according to the explanation in chapter 3 are described. Since the guided waves are excited outside the liquid and the propagation velocities of symmetric and antisymmetric modes are different, these modes arrive at different times at the water surface. Furthermore, since the piezoelectric transducer is glued a little bit apart

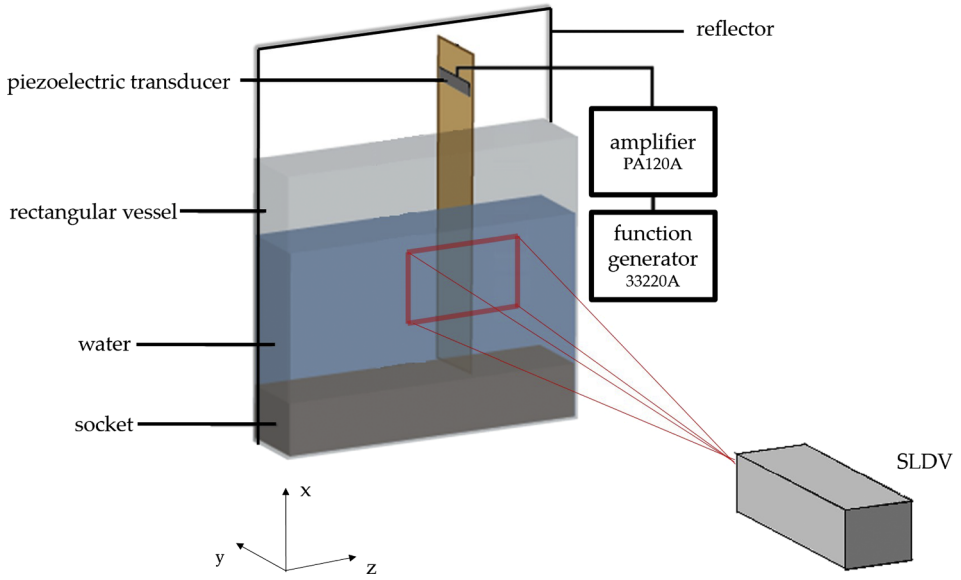

Fig. 1. Experimental set-up for the detection of the interaction of guided acoustic waves with the liquid by LRV.

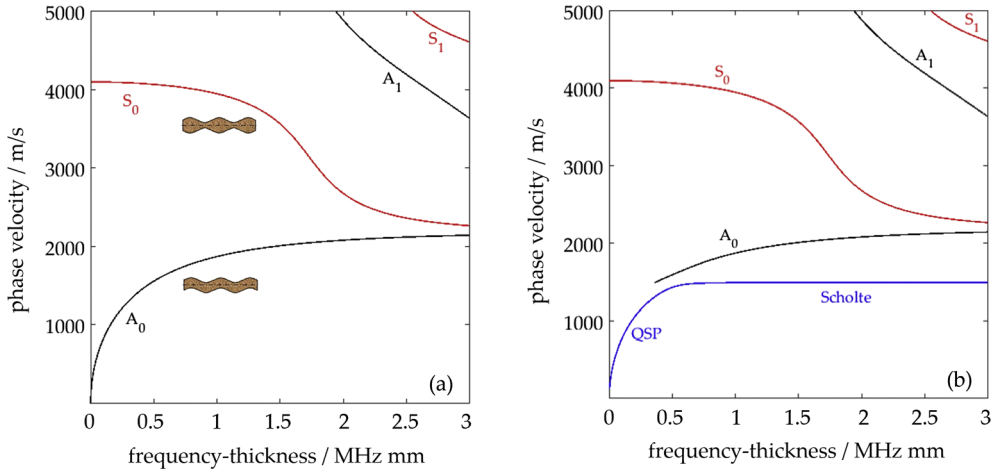

Fig. 2. Phase velocity diagram for a copper plate ($E = 132\,\text{GPa}$, $\rho = 8940\,\frac{\text{kg}}{\text{m}^3}$, $\nu = 0.3496$) in air (**a**) and immersed in water ($c_f = 1500\frac{m}{s}$, $\rho_f = 1000\,\frac{\text{kg}}{\text{m}^3}$) (**b**).

from the upper edge of the copper plate, waves reflected from the upper edge will also travel downwards into the liquid, but with some delay compared to the direct waves. Nevertheless the sequential time series of LRV records for a frequency-thickness product of 450 kHz mm shown in Fig. 4 clearly reveal the existence and behavior of different modes. Within a frame extended 10 mm each to the left and right from the central copper plate a 25 mm long downward section along the wave propagation direction is shown in each slide. The waves propagate from

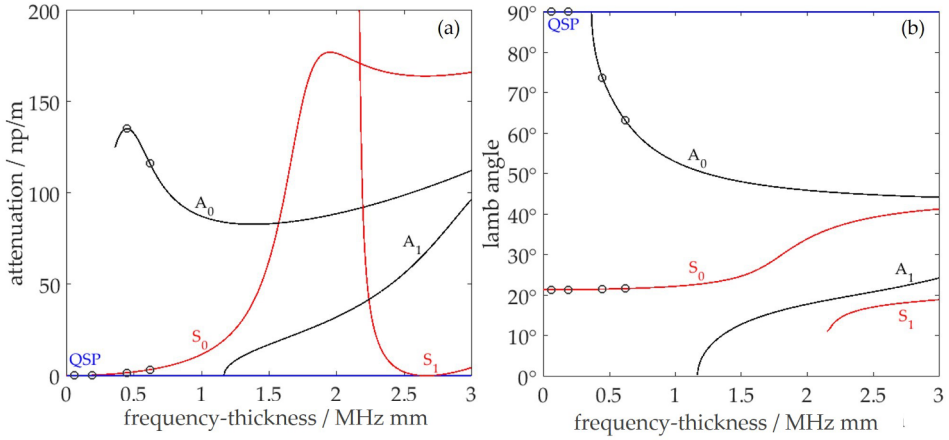

Fig. 3. Attenuation diagram for guided acoustic waves on a copper plate in water (**a**) and resulting Lamb angle (**b**).

Table 2
Results of LDV measurements at the copper plate surface in air: Perpendicular displacements of the fundamental Lamb modes at different frequency-thickness products and excitation voltages needed for a displacement of 2 nm of the A_0 mode. (n.d.: non detectable).

Lamb mode	60 kHz mm	190 kHz mm	450 kHz mm	620 kHz mm
S_0	n. d.	3.2 nm	0.6 nm	0.1 nm
A_0	51.8 nm	19.3 nm	5.3 nm	1.8 nm
exitation voltage (for 2 nm)	3.2 V_{pp}	10.4 V_{pp}	45 V_{pp}	105 V_{pp}

the upper side to the lower side. At 139.3 μs the first pressure variation in the water is recorded, which increases in amplitude until 150.2 μs. The wavefronts propagate in the water at a skew angle but also downwards along the whole length of the observed section of the plate. This wave mode is assigned to the S_0 mode, because of the rather small radiation angle and the long persistence downwards the copper plate indicating small attenuation. Later, beginning at 222.8 μs another pressure variation next to the substrate appears. This is followed by pressure variations at 231.6 μs in the water distant from the plate with skew wavefronts. The wavefronts tethered to the substrate are attributed to the QSP and the skew wavefronts radiated off the substrate to the A_0 mode. This assignment is corroborated by the increasing separation of the wavefronts of this mode from the plate with time (see e.g. at 237.4 μs), which indicates larger attenuation compared to the S_0 mode as predicted from Fig. 3. In contrast the pressure variation which is assigned to the QSP propagates without any radiation into the liquid and thereby shows no attenuation. A further confirmation of this interpretation is obtained by taking a closer look at the phase of the pressure variation to the right and left of the center of the plate. In the symmetrical mode the phase of the pressure variation is the same, whereas in the antisymmetrical or QSP mode the pressure variation is in opposite phases on both sides of the plate. For the identification of the guided acoustic wave modes the Lamb angles as well as the wavelengths of the different wave modes are extracted from the records of the LRV. For better analysis the scanning area is increased to 60 mm × 40 mm. But only the part left of the center of the plate is investigated. For the determination of the Lamb angles the maxima of the radiated waves are identified along a wavefront at a certain point in time, see Fig. 5a, b. Using the least square method, the spatial slope of a corresponding regression line was determined, from which the Lamb angle was calculated. The wavelengths of the guided acoustic waves are obtained from the spatial period of the pressure variations in a distance of approximately 0.5 mm from the plate surface at a given time instant. For example, in Fig. 5c the maxima of the fundamental symmetric mode are identified at the time 63.6 μs. On the other hand when the fundamental antisymmetric mode gets in contact with the water it is assumed that the first five periods are a mixture of the QSP and antisymmetric mode, see Fig. 5d at the time 76.3 μs. This enables an estimation of the wavelength of the antisymmetric mode. Later at 98.4 μs the A_0 mode is completely converted to a compressional wave and only the QSP mode remains tethered to the copper plate and can be analyzed, see Fig. 5e. In this way not only the wavelengths of the S_0, A_0 and QSP modes could be determined quantitatively, but also the standard deviations of these values were obtained from the regression analysis. The results of the measured and theoretically calculated wavelengths and Lamb angles for different frequency-thickness products are compiled in Table 3. The sample with the frequency-thickness product of 450 kHz mm differs from the other samples, since the measurements were performed with a frequency of 900 kHz at a 0.5 mm thick copper plate, whereas a 1 mm copper plate was used in the other cases. Irrespective of this difference the values of theoretically and experimentally determined wavelengths were in satisfying agreement. This is valid as well for the Lamb angles of the S_0 mode, whereas the values of the A_0 mode differed significantly. A closer look at Fig. 5b reveals, however, that the wavefronts of the A_0 mode are not ideal straight lines, but showed a slight bending, which makes the determination of the Lamb angle dependent of the choice of the wavefront section. Therefore, the difference between the theoretical and experimental values seems to be an artefact of the evaluation process. Besides the wavelengths and the Lamb angles the amplitudes of the pressure variations of the radiated waves and the QSP in the liquid may vary with the frequency-thickness product, which can be extracted from the LRV records as well. Such records are displayed in Fig. 6 for the S_0, A_0 and QSP modes obtained from the right side of the copper plate. In order to be able to compare the amplitudes in the liquid at different frequency-thickness products directly, in each case the excitation voltage of the transducer was chosen so as to obtain a maximum displacement of 2 nm in the A_0 mode in air according to Table 2. Due to large differences in the pressure amplitudes the colorbars for the pressure variations had to be adopted in each case. For the S_0 mode, however, the differences in the pressure variations between the

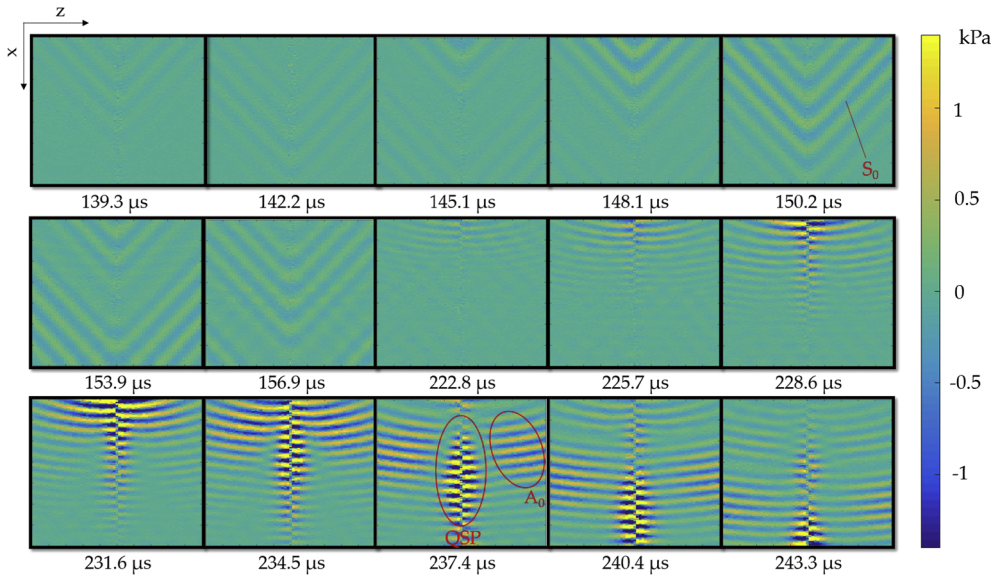

Fig. 4. LRV records of an acoustic wave pulse transmitting at 450 kHz mm from the upper side of the slide through the water at different instants of time. The frame of the pictures corresponds to extensions of 25 mm × 10 mm. Between t = 139 μs and t = 160 μs the radiating S_0 mode can be observed only. From t = 222.8 μs on the radiated A_0 mode and additionally the QSP, which is tethered to the plate, can be observed.

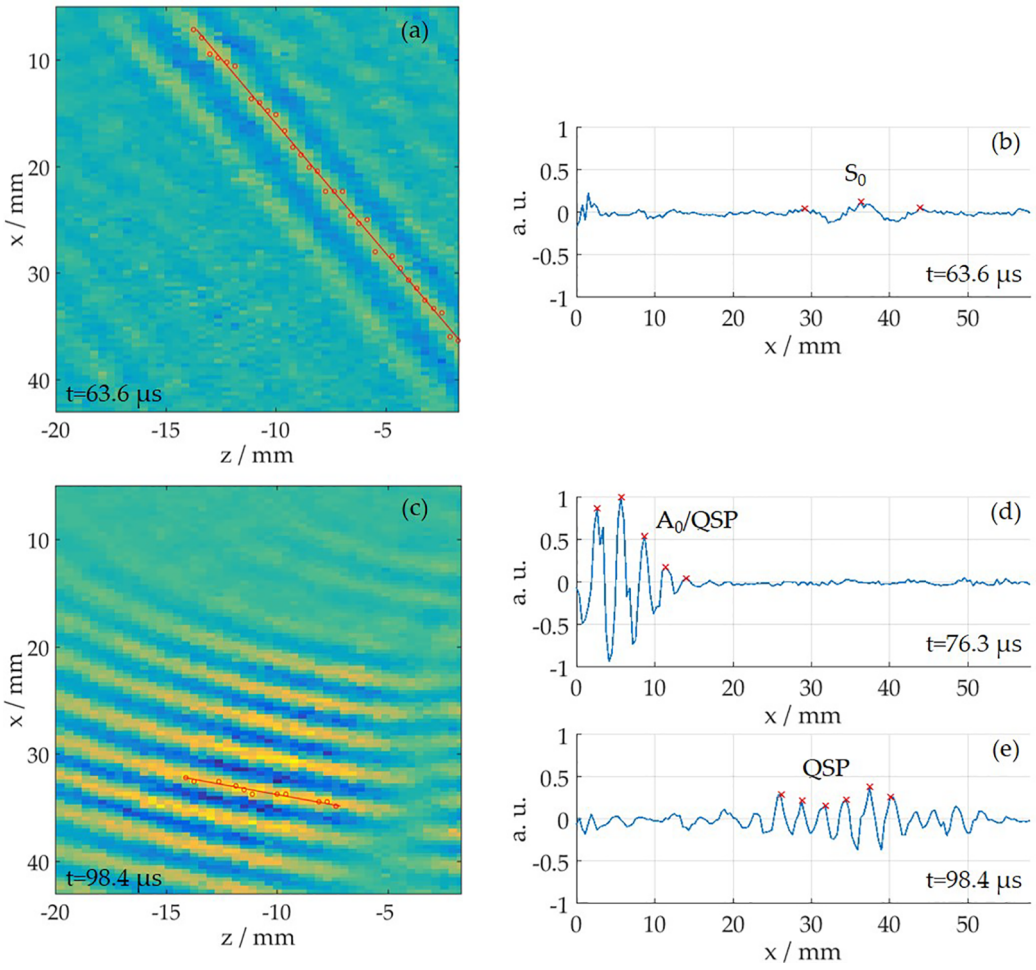

Fig. 5. Exemplary representation of the evaluation procedure for the determination of the Lamb angle by maximum search along the wavefront and determination of the slope of the wavefront for the S_0 mode (**a**) and the A_0 mode (**b**). Furthermore the evaluation of the wavelength by a maximum search and spatial period determination for the S_0 mode (**c**), the A_0 / QSP mode (**d**) and the QSP mode (**e**) at z = 0.5 mm is displayed. The measurements shown here refer to the sample with the frequency-thickness product of 620 kHz mm.

Table 3
Compilation of the theoretically and experimentally determined wavelengths and Lamb angles.

Mode	Frequency – thickness	$\lambda_{theoretical}$	$\lambda_{experimental}$	$\Theta_{theoretical}$	$\Theta_{experimental}$
S_0	60 kHz mm	68.4 mm	–	21.5°	22.6° ± 0. 7°
S_0	190 kHz mm	21.6 mm	21.7 mm ± 7.9 mm	21.5°	22.2° ± 0. 8°
S_0	450 kHz mm	4.5 mm	4.9 mm ± 0.6 mm	21.6°	22.7° ± 2. 7°
S_0	620 kHz mm	6.5 mm	6.8 mm ± 0.6 mm	21.7°	22.3° ± 0. 2°
QSP	60 kHz mm	10 mm	10.1 mm ± 1.8 mm	0°	–
QSP	190 kHz mm	5.4 mm	6.2 mm ± 0.6 mm	0°	–
QSP	450 kHz mm	1.6 mm	1.8 mm ± 0.3 mm	0°	–
QSP	620 kHz mm	2.4 mm	2.9 mm ± 0.3 mm	0°	–
A_0	450 kHz mm	1.7 mm	1.8 mm ± 0.0 mm	73.8°	64.1° ± 2. 4°
A_0	620 kHz mm	2.7 mm	2.8 mm ± 0.2 mm	63.3°	69.3° ± 1. 3°

individual frequency-thickness products are much smaller than for the A_0 and QSP modes. In general there is an increase of the amplitudes of the pressure variations of the waves in the liquid observable, which is much stronger for the A_0 and QSP modes than for the S_0 mode with increasing frequency-thickness products. At 620 kHz mm the amplitudes of the pressure fluctuations of the A_0 and QSP modes are more than ten times larger than at 60 kHz mm. In particular at low values of the frequency-thickness product the quality of the records is deteriorated by noise causing pixelated images and additionally by interferences with reflected waves from the vessel walls, e.g. in the record of the A_0 and QSP waves at 60 kHz mm. But the main features of the propagation of the different modes remain recognizable.

5. Discussion

As demonstrated by Figs. 4–6 it was possible to detect and to identify all possible wave modes arising from guided acoustic waves in a liquid in the chosen regime of the frequency-thickness product by light refractive vibrometry. Moreover, this method allows a quantitative determination of wavelengths, Lamb angles and pressure variation amplitudes. With respect to the wavelengths, the values obtained from the LRV records are in agreement with theoretical predictions based on DISPERSE calculations, see Table 3. The same holds for the Lamb angles of the S_0 modes, whereas significant deviations were obtained for the A_0 Lamb angles. These deviations are attributed to the observed bending of the wavefronts of the radiated A_0 waves, see e. g. Fig. 5. This complicates the choice of an appropriate regression line, from whose slope the Lamb angle is calculated. The tethering of the QSP to the copper plate, however, its evanescent character and its antisymmetric phase relation between both surfaces of the plate is convincingly demonstrated by Fig. 4. Moreover, the observed strong increase of the amplitudes of the pressure variations of the QSP mode with increasing frequency-thickness product can be explained by the normalized energy distribution of the QSP mode obtained from DISPERSE calculations, which is shown in Fig. 7. It can be seen that with increasing frequency-

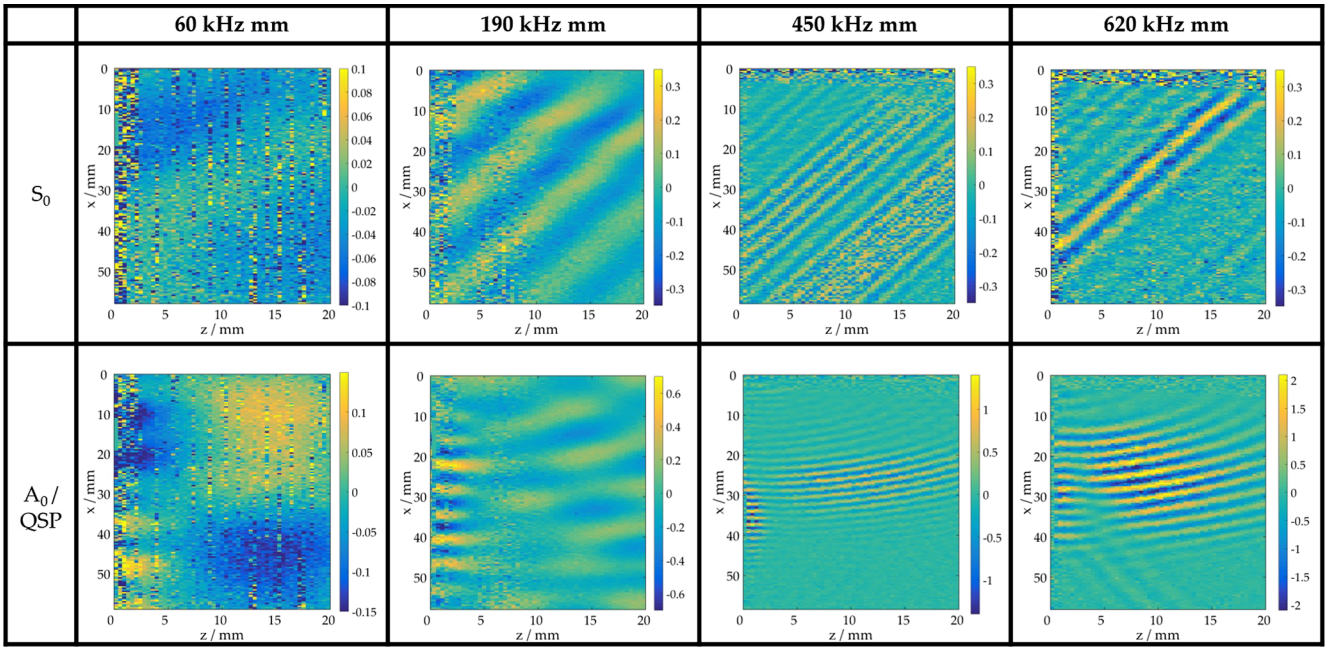

Fig. 6. LRV records of an acoustic wave pulse in the liquid with radiating S_0 (above) and A_0 (below) modes and the non-radiating QSP mode at different values of the frequency-thickness product. The colorbars indicate the pressure variations in kPa. (For interpretation of the references to colour in this figure legend, the reader is referred to the web version of this article.)

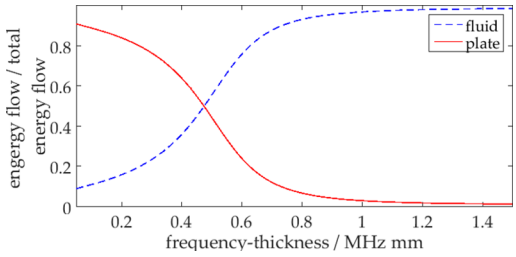

Fig. 7. Normalized energy flow of a QSP in fluid (blue dotted) and in the plate (red line). (For interpretation of the references to colour in this figure legend, the reader is referred to the web version of this article.)

thickness product more energy of the wave propagates in the fluid (blue dotted line), whereas the energy fraction in the plate decreases (red line). The observed magnitudes and changes of the amplitudes of the A_0 and S_0 modes can be explained as well with the dependence of their attenuation coefficients from the frequency-thickness product displayed in Fig. 3a. According to the DISPERSE calculation, the attenuation of the A_0 mode should be stronger than that of the S_0 mode. This results in larger amplitudes of the radiated waves and shorter propagation lengths on the copper plate for the A_0 mode, which is confirmed by the LRV records of Fig. 4 and Fig. 6. These records additionally corroborate the theoretical prediction of a maximal attenuation of the A_0 mode near a frequency-thickness product of 500 kHz mm, Fig. 3a. Correspondingly at 450 kHz mm the A_0 and the QSP are better separated than at 190 kHz mm and at 620 kHz mm (Fig. 6) indicating the strongest attenuation of the A_0 mode at 450 kHz mm. In particular with respect to quasi-Scholte plate waves, the LRV records reported herein complement the present knowledge about solid-liquid interface waves. Evidence for the existence of Scholte waves was already provided by various methods in the past. Glorieux and co-workers used the deflection of a focused laser beam reflected from the solid-liquid interface to detect Scholte wave pulses excited by laser pulses via the thermoelastic effect and to measure their velocity [39,40]. DeBilly and co-workers excited Scholte waves with piezoelectric transducers and detected them with pulse-echo or time-of-flight techniques, which allowed a determination of their velocity [10,41]. Aubert et al. visualized the evanescent field of a standing quasi-Scholte plate mode and a Scholte wave with schlieren optical measurements [14]. Due to continuous excitation, however, they were not able to study the generation and propagation of these waves in time. An approach based on LRV, which allows the visualization of a propagating interface wave in the liquid, has been chosen by Han et al. [42]. However, they measured the sound wave induced oscillations of the refractive index in the liquid at a fixed distance of 0.1 mm from the sample in the liquid. Therefore they could not follow up the distribution of the wave in the liquid; in particular, they could not determine the penetration depth of this evanescent wave mode. Summarizing, in contrast to the present state of art, the new method presented in this study based on scanning laser refractive vibrometry not only allows the temporal follow-up of the mode conversion of antisymmetric Lamb waves into quasi-Scholte plate waves at a solid-liquid interface and their propagation but also displays the extension of this evanescent wave within the liquid in a two-dimensional image.

6. Conclusion and outlook

The feasibility of the visualization of the interaction of guided acoustic waves with liquids by light refractive vibrometry is demonstrated, which will provide a comprehensive understanding of the behavior of such waves in a liquid environment. For the first time the propagation of the quasi-Scholte plate mode in the liquid has been visualized two-dimensionally in the sagittal plane. The latter is of particular importance with respect to applications of this mode for the sensing of processes and generation of streaming near solid-liquid interfaces. Examples in this respect are electrochemical transport processes, where QSP modes are supposed to play a crucial role in the enhancement of ion transport rates across the electrode-electrolyte boundary by guided acoustic waves [9,15,43].

Acknowledgments

The authors would like to thank the team of the Institute of Sensor and Actuator Technology and Martin Gamble. The support of this research by the European Fund of Regional Development (EFRE) within

the project 'InnoTerm' and by 'Technologieallianz Oberfranken (TAO)' is gratefully acknowledged.

References

[1] J.L. Rose, Ultrasonic Guided Waves in Solid, Media, Cambridge University Press, New York, 2014, https://doi.org/10.1017/CBO9781107273610.

[2] V. Giurgiutiu, Structural Health Monitoring with Piezoelectric Wafer Active Sensors, second ed., Elsevier/Academic Press, Amsterdam and Boston, 2014, https://doi.org/10.1016/B978-0-12-418691-0.00003-4.

[3] F.B. Cegla, Ultrasonic waveguide sensors for fluid characterisation and remote sensing, Ph.D. thesis, University of London, 2006.

[4] F.B. Cegla, P. Cawley, M.J.S. Lowe, Fluid bulk velocity and attenuation measurements in non-newtonian liquids using a dipstick sensor, Meas. Sci. Technol. 17 (2) (2006) 264–274, https://doi.org/10.1088/0957-0233/17/2/006.

[5] M. Schmitt, K. Schmidt, S. Olfert, J. Rautenberg, G. Lindner, B. Henning, L.M. Reindl, Detection of coatings within liquid-filled tubes and containers by mode conversion of leaky lamb waves, J. Sens. Sens. Syst. 2 (1) (2013) 73–84, https://doi.org/10.5194/jsss-2-73-2013.

[6] S. Tietze, F. Singer, S. Lasota, S. Ebert, J. Landskron, K. Schwuchow, K.S. Drese, G. Lindner, Monitoring of soft deposition layers in liquid-filled tubes with guided acoustic waves excited by clamp-on transducers, Sensors (Basel, Switzerland) 18(2). doi:https://doi.org/10.3390/s18020526.

[7] M. Wiklund, R. Green, M. Ohlin, Acoustofluidics 14: applications of acoustic streaming in microfluidic devices, Lab Chip 12 (14) (2012) 2438–2451, https://doi.org/10.1039/c2lc40203c.

[8] J. Friend, L.Y. Yeo, Microscale acoustofluidics: microfluidics driven via acoustics and ultrasonics, Rev. Modern Phys. 83 (2) (2011) 647–704, https://doi.org/10.1103/RevModPhys. 83.647.

[9] S. Tietze, J. Schlemmer, G. Lindner, Influence of surface acoustic waves induced acoustic streaming on the kinetics of electrochemical reactions, Proc. SPIE 8923 (2013) 89231B, https://doi.org/10.1117/12.2033694.

[10] M.d. Billy, G. Quentin, Experimental study of the scholte wave propagation on a plane surface partially immersed in liquid, J. Appl. Phys. 54 (8) (1983) 4314–4322, https://doi.org/10.1063/1.332666.

[11] G.D. Meegan, M.F. Hamilton, Y.A. Il'inskii, E.A. Zabolotskaya, Nonlinear stoneley and scholte waves, J. Acoust. Soc. Am. 106 (4) (1999) 1712–1723, https://doi.org/10.1121/1.427920.

[12] C. Glorieux, K. van de Rostyne, K. Nelson, W. Gao, W. Lauriks, J. Thoen, On the character of acoustic waves at the interface between hard and soft solids and liquids, J. Acoust. Soc. Am. 110 (3) (2001) 1299–1306.

[13] F.B. Cegla, P. Cawley, M.J.S. Lowe, Material property measurement using the quasi-scholte mode—a waveguide sensor, J. Acoust. Soc. Am. 117 (3) (2005) 1098–1107, https://doi.org/10.1121/1.1841631.

[14] V. Aubert, R. Wunenburger, T. Valier-Brasier, D. Rabaud, J.-P. Kleman, C. Poulain, A simple acoustofluidic chip for microscale manipulation using evanescent scholte waves, Lab Chip 16 (13) (2016) 2532–2539, https://doi.org/10.1039/c6lc00534a.

[15] S. Tietze, M. Reißenweber, J. Schlemmer, G. Lindner, Investigation of the surface condition of an electrode after electropolishing under the influence of surface acoustic waves, Phys. Proc. 70 (2015) 1039–1042, https://doi.org/10.1016/j.phpro.2015.08.221.

[16] S. Tietze, G. Lindner, Acoustic boosting of battery charging, Proc. Actuat. 16 (2016) 451–454.

[17] F.B. Cegla, Energy concentration at the center of large aspect ratio rectangular waveguides at high frequencies, J. Acoust. Soc. Am. 123 (6) (2008) 4218–4226, https://doi.org/10.1121/1.2908273.

[18] Z. Tian, L. Yu, Lamb wave frequency–wavenumber analysis and decomposition, J. Intell. Mater. Syst. Struct. 25 (9) (2014) 1107–1123, https://doi.org/10.1177/1045389X14521875.

[19] G.S. Settles, Schlieren and Shadowgraph Techniques: Visualizing Phenomena in Transparent Media, Experimental Fluid Mechanics, Springer, Berlin, 2006.

[20] M. Schmitt, S. Olfert, J. Rautenberg, G. Lindner, B. Henning, L.M. Reindl, Multi reflection of lamb wave emission in an acoustic waveguide sensor, Sens. (Basel, Switzerland) 13 (3) (2013) 2777–2785, https://doi.org/10.3390/s130302777.

[21] M. Schmitt, S. Tietze, W. Liang, G. Lindner, Measurement of the emission of lamb waves by a pvdf membrane hydrophone, AIP Conf. Proc. 615 (1433) (2012) 133–136, https://doi.org/10.1063/1.3703155.

[22] V. Wilkens, W. Molkenstruck, Broadband pvdf membrane hydrophone for comparisons of hydrophone calibration methods up to 140 mHz, IEEE Trans. Ultrason. Ferroelectr. Freq. Control 54 (9) (2007) 1784–1791, https://doi.org/10.1109/TUFFC.2007.462.

[23] B. Schneider, K.K. Shung, Quantitative analysis of pulsed ultrasonic beam patterns using a schlieren system, IEEE Trans. Ultrason. Ferroelectr. Freq. Control 43 (6) (1996) 1181–1186, https://doi.org/10.1109/58.542062.

[24] G.R. Harris, Hydrophone measurements in diagnostic ultrasound fields, IEEE Trans. Ultrason. Ferroelectr. Freq. Control 35 (2) (1988) 87–101, https://doi.org/10.1109/58.4157.

[25] R. Malkin, T. Todd, D. Robert, A simple method for quantitative imaging of 2d acoustic fields using refracto-vibrometry, J. Sound Vib. 333 (19) (2014) 4473–4482, https://doi.org/10.1016/j.jsv.2014.04.049.

[26] E. Olsson, Selective imaging of sound sources in air using phase-calibrated multi-wavelength digital holographic reconstructions, Opt. Eng. 46 (7) (2007), https://doi.org/10.1117/1.2752826 075801.

[27] I. Solodov, D. Döring, G. Busse, Air-coupled laser vibrometry: analysis and applications, Appl. Opt. 48 (7) (2009) C33, https://doi.org/10.1364/AO.48.000C33.

[28] L. Zipser, H.-D. Seelig, H. Franke, Refracto-vibrometry for visualizing ultrasound in small-sized channels, cavities and objects, International Ultrasonics Symposium, 2009, pp. 2588–2591, , https://doi.org/10.1109/ULTSYM.2009.5441537.

[29] L. Bahr, R. Lerch, Beam profile measurements using light refractive tomography, IEEE Trans. Ultrason. Ferroelectr. Freq. Control 55 (2) (2008) 405–414, https://doi.org/10.1109/TUFFC.2008.658.

[30] L. Chen, S.J. Rupitsch, R. Lerch, Noninvasive measurement of pressure fields arising from arbitrarily-shaped ultrasound transducers, 16, GMA/ITG-Fachtagung Sensor. Messsyst. 2012 (2012) 361–367, https://doi.org/10.5162/SENSOREN2012/3.3.4.

[31] K.G. Foote, P.D. Theobald, Acousto-optic effect compensation for optical determination of the normal velocity distribution associated with acoustic transducer radiation, J. Acoust. Soc. Am. 138 (3) (2015) 1627–1636, https://doi.org/10.1121/1.4929372.

[32] A.R. Harland, J.N. Petzing, J.R. Tyrer, Nonperturbing measurements of spatially distributed underwater acoustic fields using a scanning laser doppler vibrometer, J. Acoust. Soc. Am. 115 (1) (2004) 187–195, https://doi.org/10.1121/1.1635841.

[33] R. Longo, S. Vanlanduit, G. Arroud, P. Guillaume, Underwater acoustic wavefront visualization by scanning laser doppler vibrometer for the characterization of focused ultrasonic transducers, Sens. (Basel, Switzerland) 15 (8) (2015) 19925–19936, https://doi.org/10.3390/s150819925.

[34] Y. Wang, J. Tyrer, P. Zhihong, W. Shiquan, Measurement of focused ultrasonic fields using a scanning laser vibrometer, J. Acoust. Soc. Am. 121 (5) (2007) 2621–2627, https://doi.org/10.1121/1.2713708.

[35] I.A. Viktorov, Rayleigh and Lamb Waves: Physical Theory and Applications, Ultrasonic Technology, Springer, US, Boston, 1967.

[36] T. Kundu (Ed.), Ultrasonic Nondestructive Evaluation: Engineering and Biological Material Characterization, CRC Press, Boca Raton, Fla, 2004.

[37] A. Lewin, F. Mohr, H. Selbach, Heterodyn-interferometer zur vibrationsanalyse, tm – Techn. Messen 57 (9) (1990) 335–439, https://doi.org/10.1524/teme.1990.57.jg.335.

[38] C.B. Scruby, L.E. Drain, Laser Ultrasonics: Techniques and Applications, A. Hilger, Bristol, England and Philadelphia, 1990.

[39] C. Glorieux, K. van de Rostyne, J.D. Beers, W. Gao, S. Petillion, N. van Riet, K.A. Nelson, J.F. Allard, V.E. Gusev, W. Lauriks, J. Thoen, Acoustic waves at interfaces studied by laser ultrasonics (invited), Rev. Sci. Instrum. 74 (1) (2003) 465–469, https://doi.org/10.1063/1.1512978.

[40] C. Desmet, V. Gusev, W. Lauriks, C. Glorieux, J. Thoen, All-optical excitation and detection of leaky rayleigh waves, Opt. Lett. 22 (2) (1997) 69–71, https://doi.org/10.1364/OL.22.000069.

[41] M.d. Billy, I. Molinero, On the nonobservance of nonspecular bounded beam reflection effects of lamb modes, J. Acoust. Soc. Am. 83 (4) (1988) 1249–1254, https://doi.org/10.1121/1.395980.

[42] Q. Han, M. Qian, H. Wang, Investigation of liquid-solid interface waves with laser excitation and photoelastic effect detection, J. Appl. Phys. 100 (9) (2006), https://doi.org/10.1063/1.2365377 093101.

[43] O. Dubrovski, S. Tietze, A. Zigelman, K.S. Drese, G. Lindner, O. Manor, Editors' choice—the enhancement of ion transport in an electrochemical cell using high frequency vibration for the electropolishing of copper, J. Electrochem. Soc. 165 (5) (2018) E236–E244, https://doi.org/10.1149/2.0811805jes.